Probing Electron-Phonon Interaction through Two-Photon Interference in Resonantly Driven Semiconductor Quantum Dots

Antoine Reigue,[1] Jake Iles-Smith,[2,*] Fabian Lux,[1] Léonard Monniello,[1] Mathieu Bernard,[1] Florent Margaillan,[1]
Aristide Lemaitre,[3] Anthony Martinez,[3] Dara P. S. McCutcheon,[4] Jesper Mørk,[2] Richard Hostein,[1] and Valia Voliotis[1,†]

[1]*Sorbonne Universités, UPMC Université Paris 06, CNRS UMR 7588, Institut des NanoSciences de Paris, F-75005 Paris, France*
[2]*Department of Photonics Engineering, DTU Fotonik, Ørsteds Plads, 2800 Kongens Lyngby, Denmark*
[3]*Centre de Nanosciences et de Nanotechnologies, CNRS, Université Paris-Sud,
Université Paris-Saclay, 91460 Marcoussis, France*
[4]*Quantum Engineering Technology Labs, H. H. Wills Physics Laboratory and Department of Electrical and Electronic Engineering,
University of Bristol, Merchant Venturers Building, Woodland Road, Bristol BS8 1FD, United Kingdom*
(Received 21 December 2016; published 6 June 2017)

We investigate the temperature dependence of photon coherence properties through two-photon interference (TPI) measurements from a single quantum dot (QD) under resonant excitation. We show that the loss of indistinguishability is related only to the electron-phonon coupling and is not affected by spectral diffusion. Through these measurements and a complementary microscopic theory, we identify two independent separate decoherence processes, both of which are associated with phonons. Below 10 K, we find that the relaxation of the vibrational lattice is the dominant contribution to the loss of TPI visibility. This process is non-Markovian in nature and corresponds to real phonon transitions resulting in a broad phonon sideband in the QD emission spectra. Above 10 K, virtual phonon transitions to higher lying excited states in the QD become the dominant dephasing mechanism, this leads to a broadening of the zero phonon line, and a corresponding rapid decay in the visibility. The microscopic theory we develop provides analytic expressions for the dephasing rates for both virtual phonon scattering and non-Markovian lattice relaxation.

Many recent developments in quantum information processing rely on the use of solid-state qubits that can emit indistinguishable single photons on demand [1,2]. However, maintaining the coherence between consecutively emitted photons remains a true challenge for realizing a deterministic source of identical photons. A promising candidate for the development of such a source is that of self-assembled semiconductor quantum dots (QDs) embedded in photonic nanostructures [3,4].

Despite impressive milestones in the development of these devices, a QD naturally couples strongly to its surrounding solid-state matrix, constituting an inherently open quantum system. The excitonic degrees of freedom are heavily influenced by the vibrational modes [5–8], fluctuating charges [9], and nuclear spins [10] of the host material, all of which lead to dephasing, thereby suppressing the coherence properties of the emitted photons. Decoherence may be reduced by enhancing the emission rate through the Purcell effect, or by using resonant excitation to minimize laser-induced dephasing, leading to bright single-photon sources with near unity indistinguishability [11–15].

Still, there are a number of open questions regarding the role of phonon processes on the coherence properties of emitted photons. Recent experimental and theoretical work has demonstrated the importance of a microscopic model for understanding the role of phonons in the emission properties of QDs [8,16–26]. Examples include

excitation-induced dephasing of excitonic Rabi oscillations [5,27], sideband linewidth in resonance fluorescence (RF) [21,28,29], and temperature-dependent Rabi frequency renormalization [6,21]. In the examples given, the excitonic degrees of the QD are assumed to couple linearly to the phonon environment, inducing thermalization in the QD eigenbasis [7,8], leading to a broad non-Markovian sideband in the QD emission spectra [30].

Here, we present a combined experimental and theoretical investigation of the coherence properties of photons emitted by a quantum dot, allowing us, unambiguously, to separate real and virtual decoherence processes due to phonons and their temperature dependencies. To do so, we take temperature-dependent measurements of two-photon interference (TPI) in a Hong-Ou-Mandel (HOM) configuration using strictly resonant excitation conditions. We show that TPI measurements are not affected by spectral diffusion due to fluctuating charges, as this process is slow compared to the emission time interval between the two interfering photons. Therefore, loss of indistinguishability is attributed only to electron-phonon scattering. Through temperature dependent TPI measurements, we demonstrate that linear electron-phonon coupling is not sufficient to capture the trend in TPI visibility. In order to describe the behavior observed, we develop a microscopic model, based on polaron theory, to include phonon-induced virtual transitions to higher lying states in the QD [31,32]; this
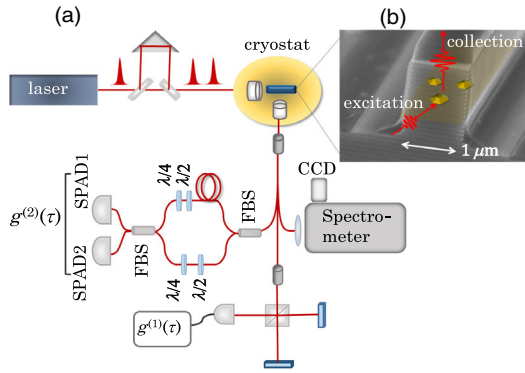
FIG. 1. (a) Scheme of the experimental setup. A tunable Ti: sapphire (82-MHz) laser delivers 3-ps pulses and, for HOM experiments, pairs of pulses separated by 3 ns. The laser is focused by a microscope objective on the cleaved edge of one ridge, and the RF is collected from the top surface by a second microscope objective. The sample and the two objectives are inside a closed-cycle He temperature-variable cryostat. The signal is coupled to a fibered setup (FBS denotes the fibered beam splitters) for either standard spectroscopy or Michelson interferometry ($g^{(1)}$) or TPI experiments ($g^{(2)}$) using a 3-ns unbalanced Mach-Zehnder interferometer. Single-photon avalanche diodes (SPAD1 and SPAD2) collect the signal. (b) Scanning electron microscopy image of one ridge, with the dots schematically drawn in the layer.

TABLE I. Values of the experimental parameters (see the text for definitions) for the three QDs under resonant excitation. $\tilde{V}$ is the expected TPI visibility from T_1 and T_2 measurements, assuming random dephasing processes (see the text).

	T_1(ps)	η	$T_2/2T_1$	$g^{(2)}_{HBT}$	V_{TPI}	$\tilde{V}$
QD1	1100	0.45	0.35	0.12	0.79	0.33
QD2	750	0.55	0.23	0.11	0.83	0.22
QD3	670	0.10	0.71	0.07	0.83	0.68
Errors	2%	±0.1	10%–15%	±0.02	±0.04	10%–15%

Second-order correlation measurements have been performed, allowing a characterization of the single-photon emission purity and indistinguishability. Figure 2 shows the results obtained for QD1 at 4 K. Single-photon interferences in a Hanbury Brown–Twiss (HBT) experiment [Fig. 2(a)] clearly show an antibunching with a low multiphoton probability $g^{(2)}_{HBT}$; the values are given for the three QDs in Table I. We attribute the background correlations at 0- and ±3-ns delay to the remaining scattered laser. The unusual shape of the histogram of coincidences is explained by the fact that the single photons pass through the two arms of the Mach-Zehnder interferometer used for the HOM setup [see Fig. 1(a) and Ref. [38]]. A multiexponential decay fit (the red line) is used to extract the value of $g^{(2)}_{HBT}$, taking into account the overlapping of the different peaks. Figure 2(b) shows the raw histogram of the TPI coincidences for QD1 at 4 K. The signature of the indistinguishability of two successively emitted photons corresponds to the small area of peak 2 compared to peaks 1 and 3. The TPI visibility V_{TPI} (see Table I) is deduced from the second-order correlation function at zero delay $g^{(2)}_{HOM}$ corrected by the remaining scattered laser and by the experimental imperfections (contrast of the Mach-Zehnder interferometer and not perfect 50:50 fibered beam splitters) [38,40].

In the literature, it is commonly accepted that the visibility of TPI experiments can be obtained from the ratio $T_2/2T_1$, assuming random dephasing processes by phonons and charges [41], and this visibility is labeled $\tilde{V}$ hereafter.

leads to temperature-dependent broadening of the zero phonon line (ZPL). Our formalism allows us to derive analytic forms for the dephasing due to both virtual phonon processes and non-Markovian lattice relaxation. This provides novel insights into the dephasing mechanisms relevant to QD based single-photon sources.

Experiment.—In contrast to previous temperature-dependent TPI measurements [33], our geometry (see Fig. 1) [34] allows us to use strictly resonant (*s*-shell) excitation removing dephasing due to relaxation from higher excited states and time jitter [35]. Furthermore, the only filtering used in our measurements is due to a low-Q cavity, which increases the collection efficiency. We present results on three different self-assembled InAs/GaAs QDs from different samples (labeled QD1, QD2, and QD3 hereafter) excited with resonant π pulses. Depending on the QD under study, an additional very weak (few nanowatt) He-Ne laser is added to enhance or recover the RF, as reported previously [15,36,37]. Experimental details can be found in the Supplemental Material [38].

The coherence time T_2, which corresponds to the width of the RF line, can be measured by Fourier transform (FT) spectroscopy using a Michelson interferometer. The contrast of the interference fringes is adjusted by a pseudo-Voigt profile, with an inhomogeneous contribution η (see Ref. [38]) that is usually attributed to spectral diffusion effects [39]. In Table I we give the values of the measured radiative lifetime T_1 of η and the ratio $T_2/2T_1$ for the three QDs. The corresponding FT spectra for the three QDs are given in Fig. 2 of the Supplemental Material [38].

FIG. 2. Second-order correlation measurements for QD1 at 4 K for a 1-hr acquisition time. (a) Coincidences histogram for the HBT experiment. We extract $g^{(2)}_{HBT} = 0.12 \pm 0.02$. (b) Coincidences histogram for the TPI experiment. After correction by the remaining laser background, we obtain $V_{TPI} = 0.79 \pm 0.03$.

The values of $\tilde{V}$ are given in Table I and correspond to a poor degree of indistinguishability. This is in striking contrast to the results obtained by TPI experiments, where $V_{\text{TPI}} \sim 0.80$ for all QDs at 4 K. The significant difference can be explained by recognizing the distinct characteristic time scales of the two kinds of experiments, which probe different physical dephasing processes [11,12,33,42,43]. Indeed, because of the long acquisition time (seconds) during T_2 measurements, the visibility $\tilde{V}$ integrates the interaction processes with the acoustic phonon bath (picosecond range) and the electrostatic environment (microsecond range [44]). By contrast, TPI experiments have a characteristic time scale defined by the nanosecond time delay between pulses; therefore, only the QD-acoustic phonon interactions are probed, thus leading to a much higher visibility. This is corroborated by the inhomogeneous contribution η, which is large when the interaction between the QDs and the charges is dominant [39] and corresponds then to a low value of $\tilde{V}$. At variance with our results, it has been recently reported that TPI experiments probe both charge fluctuations and phonon-induced dephasing [11,33]. However, in these experiments a nonresonant excitation has been used, explaining a probable laser-induced dephasing. Moreover, very recently, Wang *et al.* [45] have also shown, by increasing the time delay between the emission of the two photons, that spectral diffusion has no effect (in the nanosecond range) on the visibility when the QD is resonantly pumped.

The clear separation of time scales described above means that TPI measurements effectively isolate the phonon processes from other dephasing mechanisms. Thus, through temperature-dependant TPI experiments performed on a resonantly driven single QD, we can directly assess the importance of phonon processes on the coherence properties of subsequently emitted photons. The measured V_{TPI} as a function of the temperature for QD1 is presented in Fig. 3, where a clear loss of indistinguishability around 10 K is observed. To describe this behavior
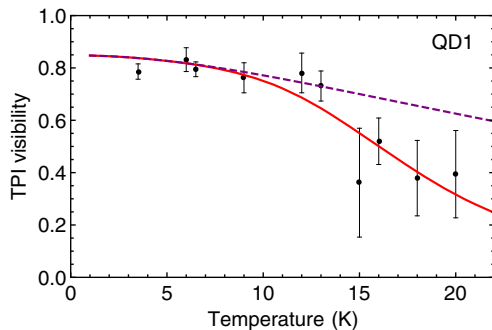
FIG. 3.   Plot showing the visibility of the measured TPI for QD1 as a function of temperature (the black points). The data are fitted with Eq. (2); the full expression is used to produced the solid red curve, which fits accurately over the full temperature range. The dashed purple curve shows only the effect of the phonon sideband on the TPI visibility.

below, we develop a theoretical model which fully captures the observed trend in visibility.

Microscopic model.—In principle, the many-body electron-phonon interaction Hamiltonian contains all possible electronic configurations of the QD [46]. However, when calculating the effect of phonons on the exciton dynamics, the energy separation between the s and p orbitals of the QD is typically a few tens of meV, and it is thus significantly higher than the average phonon energies in low temperature experiments. With this in mind, any transitions from the first excited to another electronic state of the QD must be virtual in nature. Following Muljarov and Zimmermann [31] we derive an effective Hamiltonian theory [47], treating the charge density operator as a perturbation, with the first- and second-order terms capturing real and virtual phonon transitions, respectively, as shown schematically in Fig. 4.

We start by explicitly considering the ground state $|0\rangle$ and the single exciton in the s shell denoted $|X\rangle$, with excitonic splitting ω_X. By using an effective Hamiltonian theory [47], we can eliminate off diagonal transitions to higher lying phonon states [31], yielding the Hamiltonian, $H = H_0 + |X\rangle\langle X|(\hat{V} + \hat{V}_Q)$. Here, $H_0 = \omega_X|X\rangle\langle X| + \sum_{\mathbf{k}} \nu_{\mathbf{k}} b_{\mathbf{k}}^{\dagger} b_{\mathbf{k}}$ is the free Hamiltonian of the QD and phonon environment, where $b_{\mathbf{k}}$ is the annihilation operator of a phonon with wave vector $\mathbf{k}$ and frequency $\nu_{\mathbf{k}}$. The electron-phonon interaction has two contributions: the first is the standard linear electron-phonon coupling $\hat{V} = \sum_{\mathbf{k}} g_{\mathbf{k}}(b_{\mathbf{k}}^{\dagger} + b_{\mathbf{k}})$, describing the displacement of the lattice due to the change in charge configuration of the QD [8]. The coupling strength is quantified through the matrix element $g_{\mathbf{k}} = \sum_{a=e,h} M_{a,\mathbf{k}}^{11}$, where for deformation potential coupling,

$$M_{a,\mathbf{k}}^{ij} = \sqrt{\frac{\nu_{\mathbf{k}}}{2\varrho c_s^2 \mathcal{V}}} D_a \int d^3r \, \psi_{ia}^*(\mathbf{r}) \psi_{ja}(\mathbf{r}) e^{i\mathbf{k}\cdot\mathbf{r}},$$

is the matrix element corresponding to the phonon-induced transition between the ith and jth electronic states. Here, ϱ is the mass density, c_s is the speed of sound in the material, and $\mathcal{V}$ is the phonon normalization volume. This matrix element is dependent on the wave function $\psi_{i,e/h}(\mathbf{r})$ of the
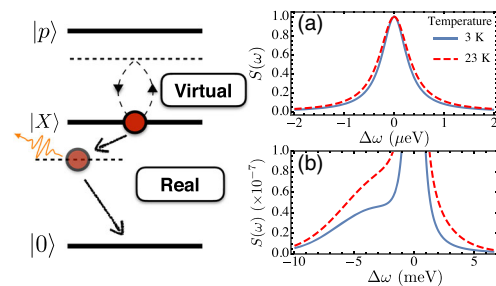
FIG. 4.   (Left panel) Schematic of real and virtual transition in a QD. (a),(b) The impact of these transitions on the QD spectra. Virtual transitions give a broadening of the ZPL as in (a). Real transitions lead to the broad phonon sideband illustrated in (b).

confined electron (e) or hole (h), and the corresponding deformation potential D_a.

The second term is quadratic in phonon operators [31] $V_Q = \sum_{\mathbf{k},\mathbf{k}'} f_{\mathbf{k},\mathbf{k}'}(b_{\mathbf{k}}^\dagger + b_{\mathbf{k}})(b_{\mathbf{k}'}^\dagger + b_{\mathbf{k}'})$, and it describes virtual phonon transitions between the first exciton state and higher lying excited states. The effective coupling strength for the quadratic coupling takes the form $f_{\mathbf{k},\mathbf{k}'} = \sum_{a=e,h} \sum_{j>1} M_{a,\mathbf{k}}^{1j} M_{a,\mathbf{k}'}^{j1} [\omega_m^a - \omega_1^a]^{-1}$, where $\omega_m^{e/h}$ is the energy of the mth electron or hole energy level.

To model the impact of the phonon processes on the photon indistinguishability, we make use of the polaron transformation [8,16,18,48] through the operator, $\mathcal{U} = |0\rangle\langle0| + |X\rangle\langle X|e^S$, where $S = \sum_{\mathbf{k}} g_{\mathbf{k}}(b_{\mathbf{k}}^\dagger - b_{\mathbf{k}})/\nu_{\mathbf{k}}$. This transformation leads to a state dependent displacement of the phonon environment, removing the linear electron-phonon coupling. Applying this transformation to our quadratic Hamiltonian, we obtain $H_V = \mathcal{U}^\dagger H \mathcal{U} = (\tilde{\omega}_X + \hat{V}_Q)|X\rangle\langle X| + \sum_{\mathbf{k}} \nu_{\mathbf{k}} b_{\mathbf{k}}^\dagger b_{\mathbf{k}}$. Notice the residual quadratic electron-phonon coupling, and that the QD resonance is shifted, $\tilde{\omega}_X = \omega_X + \sum_{\mathbf{k}} g_{\mathbf{k}}^2/\nu_{\mathbf{k}}$. From this Hamiltonian we may derive a master equation for the reduced density matrix of the QD in the polaron frame, χ, which takes the simple pure dephasing form

$$\dot{\chi}(t) = -i\tilde{\omega}_X[\sigma^\dagger\sigma, \chi(t)] + \Gamma\mathcal{L}_\sigma[\chi(t)] + 2\gamma_{\mathrm{pd}}\mathcal{L}_{\sigma^\dagger\sigma}[\chi(t)],$$

where $\sigma = |0\rangle\langle X|$ is the dipole transition operator and $\mathcal{L}_O[\chi] = O\chi O^\dagger - \{O^\dagger O, \chi\}/2$. Here, Γ is the radiative recombination rate of the QD. If we consider only virtual transitions between the lowest exciton states and the next highest states [49], we may find an analytic form for the pure dephasing rate due to the virtual phonon transition [38]:

$$\gamma_{\mathrm{pd}} = \frac{\alpha^2\mu}{\nu_c^4}\int_0^\infty \nu^{10} e^{-2\nu^2/\nu_c^2} n(\nu)(n(\nu)+1)\,d\nu, \quad (1)$$

where $n(\nu) = [e^{-\beta\nu} - 1]^{-1}$. α and μ describe the electron-phonon coupling strength and the probability of virtual phonon processes, respectively. The cutoff frequency, ν_c, is directly related to the QD confinement length.

To calculate the visibility of two-photon interference, we must associate the excitonic degrees of freedom in the QD to the emitted field. In the polaron frame, one obtains the Heisenberg picture field operator $\hat{E}(t) = \sqrt{\Gamma/2\pi}\sigma(t)B_-(t)$, where the standard expression for a dipole emitter is modified by the phonon displacement operator $B_\pm(t) = e^{\pm S(t)}$ [24,26]. With this expression we obtain the polaron frame first-order correlation function, $g^{(1)}(t,\tau) = (\Gamma/2\pi)\langle B_+(\tau)B_-\rangle\langle\sigma^\dagger(t+\tau)\sigma(t)\rangle$. The second term in this equation describes emission through the ZPL. The first term is the phonon correlation function, which takes the form $\langle B_+(\tau)B_-\rangle = B^2\exp[\varphi(\tau)]$, where $B = \exp[-\varphi(0)/2]$ is the Franck-Condon factor, and $\varphi(\tau) = \alpha\int_0^\infty \nu\exp(-\nu^2/\nu_c^2)[\coth(\beta\nu/2)\cos(\nu\tau) - i\sin(\nu\tau)]d\nu$. This

function decays on a time scale related to the inverse of the cutoff frequency, which is typically on the order of picoseconds, leading to a broad phonon sideband in the spectra of the system. A detailed derivation of this expression is given in the Supplemental Material [38].

Following Ref. [26], we obtain an analytic form for the indistinguishability including the phonon sideband contribution [38]:

$$\mathcal{I} = \frac{\Gamma}{\Gamma + 2\gamma_{\mathrm{pd}}}\left(\frac{|h(0)|^2 B^2}{|h(0)|^2 B^2 + \mathcal{F}(1-B^2)}\right)^2, \quad (2)$$

where $|h(0)|^2 = (\kappa/2)^2(\delta^2 + (\kappa/2)^2)^{-1}$, with κ being the cavity width and δ the QD-cavity detuning. The first factor gives the contribution of photons emitted through the ZPL, while the second describes the reduction of the indistinguishability from photons emitted through the phonon sideband. The temperature-dependent factor, $\mathcal{F}$, quantifies the unfiltered fraction of the phonon sideband extracted from the low-Q cavity [50].

We use the above expression to fit the experimental data given in Fig. 3, using a least mean squared fitting. We find an optimum fit for parameters $\alpha = 0.0082$ ps^2, $\nu_c = 7.9$ ps^{-1}, and $\mu = 4.4\times10^{-4}$ ps^2. α and μ depend only on the material parameters, and reasonable agreement is found upon comparison to the theoretical values. The cutoff frequency gives a characteristic confinement length on the order of 1 nm, which is the right order of magnitude for typical self-assembled QDs. The fit captures the qualitative and quantitative behavior of the data. Furthermore, from the simple form of the expression given in Eq. (2), we can analyze the contributions to the indistinguishability due to the phonon sideband, and the virtual transitions to higher lying QD states. Similar results have been obtained for QD2 and are presented in the Supplemental Material [38].

Below 10 K, the average energy of phonons $k_B T$ is not sufficient to induce virtual transitions ($\gamma_{\mathrm{pd}} \ll \Gamma$). If we use the extracted parameters to consider only the sideband contribution (the dashed curve), we observe a good fit at low temperatures, with an $\sim$10% reduction in the indistinguishability, suggesting that emission via the phonon sideband is the principal cause for the reduction of TPI visibility. However, above 10 K the data demonstrate a rapid decrease in the indistinguishability not captured by the sideband theory. At these temperatures, $k_B T$ is sufficient to induce virtual transitions between the s and p states of the QD, leading to pure dephasing of the ZPL ($\gamma_{\mathrm{pd}} \sim \Gamma$) and, consequently, a suppression of the indistinguishability.

The fact that real and virtual phonon processes occur on separate temperature scales is of vital importance to the development of solid-state single-photon sources. Although the phonon sideband is a persistent problem at low temperatures, it may be easily removed through spectral filtering, or use of a high-Q cavity [26]. Though this could reduce the

efficiency of the source, transform limited photons may be obtained as $\gamma_{pd} \approx 0$ at low temperature. By contrast, the broadening of the ZPL cannot be removed through simple filtering; instead, one must rely on Purcell enhancement to reduce its influence. However, the sensitivity of virtual phonon processes to temperature will place significant limitations on the operating regimes of QD systems.

In summary, through temperature-dependent TPI measurements, we have demonstrated that both real and virtual phonon transitions, occurring on very different time scales, play a role in reducing the indistinguishability of photons emitted from QDs under resonant excitation. Using a rigorous microscopic theory, we provide analytic expressions for the dephasing due to these mechanisms, providing new insights into potential operating regimes of QD single-photon sources. Furthermore, we expect such a general microscopic approach could be used to describe other specific discrete quantum systems coupled to a bosonic reservoir.

---

[*]jakeilessmith@gmail.com
[†]voliotis@insp.jussieu.fr

[1] A. Kiraz, M. Atatüre, and A. Imamoğlu, Phys. Rev. A **69**, 032305 (2004).

[2] S. Buckley, K. Rivoire, and J. Vučković, Rep. Prog. Phys. **75**, 126503 (2012).

[3] P. Lodahl, S. Mahmoodian, and S. Stobbe, Rev. Mod. Phys. **87**, 347 (2015).

[4] W. B. Gao, A. Imamoglu, H. Bernien, and R. Hanson, Nat. Photonics **9**, 363 (2015).

[5] A. J. Ramsay, A. V. Gopal, E. M. Gauger, A. Nazir, B. W. Lovett, A. M. Fox, and M. S. Skolnick, Phys. Rev. Lett. **104**, 017402 (2010).

[6] A. J. Ramsay, T. M. Godden, S. J. Boyle, E. M. Gauger, A. Nazir, B. W. Lovett, A. M. Fox, and M. S. Skolnick, Phys. Rev. Lett. **105**, 177402 (2010).

[7] D. P. S. McCutcheon and A. Nazir, Phys. Rev. Lett. **110**, 217401 (2013).

[8] A. Nazir and D. P. S. McCutcheon, J. Phys. Condens. Matter **28**, 103002 (2016).

[9] J. Houel, A. Kuhlmann, L. Greuter, F. Xue, M. Poggio, B. Gerardot, P. Dalgarno, A. Badolato, P. Petroff, A. Ludwig et al., Phys. Rev. Lett. **108**, 107401 (2012).

[10] A. V. Kuhlmann, J. Houel, A. Ludwig, L. Greuter, D. Reuter, A. D. Wieck, M. Poggio, and R. J. Warburton, Nat. Phys. **9**, 570 (2013); A. V. Kuhlmann, J. H. Prechtel, J. Houel, A. Ludwig, D. Reuter, A. D. Wieck, and R. J. Warburton, Nat. Commun. **6**, 8204 (2015).

[11] O. Gazzano, S. M. de Vasconcellos, C. Arnold, A. Nowak, E. Galopin, I. Sagnes, L. Lanco, A. Lemaître, and P. Senellart, Nat. Commun. **4**, 1425 (2013).

[12] X. Ding, Y. He, Z.-C. Duan, N. Gregersen, M.-C. Chen, S. Unsleber, S. Maier, C. Schneider, M. Kamp, S. Höfling et al., Phys. Rev. Lett. **116**, 020401 (2016).

[13] Y.-M. He, Y. He, Y.-J. Wei, D. Wu, M. Atatüre, C. Schneider, S. Höfling, M. Kamp, C.-Y. Lu, and J.-W. Pan, Nat. Nanotechnol. **8**, 213 (2013).

[14] N. Somaschi, V. Giesz, L. De Santis, J. Loredo, M. Almeida, G. Hornecker, S. Portalupi, T. Grange, C. Anton, J. Demory et al., Nat. Photonics **10**, 340 (2016).

[15] L. Monniello, A. Reigue, R. Hostein, A. Lemaitre, A. Martinez, R. Grousson, and V. Voliotis, Phys. Rev. B **90**, 041303 (2014).

[16] D. P. S. McCutcheon and A. Nazir, New J. Phys. **12**, 113042 (2010).

[17] M. Glässl, L. Sörgel, A. Vagov, M. D. Croitoru, T. Kuhn, and V. M. Axt, Phys. Rev. B **86**, 035319 (2012).

[18] C. Roy and S. Hughes, Phys. Rev. Lett. **106**, 247403 (2011).

[19] P. Kaer, T. R. Nielsen, P. Lodahl, A.-P. Jauho, and J. Mørk, Phys. Rev. B **86**, 085302 (2012).

[20] A. Majumdar, E. D. Kim, Y. Gong, M. Bajcsy, and J. Vučković, Phys. Rev. B **84**, 085309 (2011).

[21] Y.-J. Wei, Y. He, Y.-M. He, C.-Y. Lu, J.-W. Pan, C. Schneider, M. Kamp, S. Höfling, D. P. S. McCutcheon, and A. Nazir, Phys. Rev. Lett. **113**, 097401 (2014).

[22] I. Wilson-Rae and A. Imamoğlu, Phys. Rev. B **65**, 235311 (2002).

[23] U. Hohenester, Phys. Rev. B **81**, 155303 (2010).

[24] J. Iles-Smith, D. P. S. McCutcheon, J. Mørk, and A. Nazir, Phys. Rev. B **95**, 201305(R) (2017).

[25] J. Iles-Smith and A. Nazir, Optica **3**, 207 (2016).

[26] J. Iles-Smith, D. P. S. McCutcheon, A. Nazir, and J. Mørk, Nat. Photonics (to be published).

[27] L. Monniello, C. Tonin, R. Hostein, A. Lemaitre, A. Martinez, V. Voliotis, and R. Grousson, Phys. Rev. Lett. **111**, 026403 (2013).

[28] E. Flagg, A. Muller, J. Robertson, S. Founta, D. Deppe, M. Xiao, W. Ma, G. Salamo, and C.-K. Shih, Nat. Phys. **5**, 203 (2009).

[29] S. M. Ulrich, S. Ates, S. Reitzenstein, A. Löffler, A. Forchel, and P. Michler, Phys. Rev. Lett. **106**, 247402 (2011).

[30] P. Kaer, N. Gregersen, and J. Mork, New J. Phys. **15**, 035027 (2013); P. Kaer and J. Mørk, Phys. Rev. B **90**, 035312 (2014).

[31] E. A. Muljarov and R. Zimmermann, Phys. Rev. Lett. **93**, 237401 (2004).

[32] T. Grange, Phys. Rev. B **80**, 245310 (2009).

[33] A. Thoma, P. Schnauber, M. Gschrey, M. Seifried, J. Wolters, J.-H. Schulze, A. Strittmatter, S. Rodt, A. Carmele, A. Knorr et al., Phys. Rev. Lett. **116**, 033601 (2016).

[34] R. Melet, V. Voliotis, A. Enderlin, D. Roditchev, X. L. Wang, T. Guillet, and R. Grousson, Phys. Rev. B **78**, 073301 (2008).

[35] S. Unsleber, D. P. S. McCutcheon, M. Dambach, M. Lermer, N. Gregersen, S. Höfling, J. Mørk, C. Schneider, and M. Kamp, Phys. Rev. B **91**, 075413 (2015).

[36] H.-S. Nguyen, G. Sallen, C. Voisin, P. Roussignol, C. Diederichs, and G. Cassabois, Phys. Rev. Lett. **108**, 057401 (2012).

[37] H. S. Nguyen, G. Sallen, M. Abbarchi, R. Ferreira, C. Voisin, P. Roussignol, G. Cassabois, and C. Diederichs, Phys. Rev. B **87**, 115305 (2013).

[38] See Supplemental Material at http://link.aps.org/supplemental/10.1103/PhysRevLett.118.233602 for more details about the experimental setup, data analysis, additional results and theoretical calculations.

[39] A. Berthelot, I. Favero, G. Cassabois, C. Voisin, C. Delalande, P. Roussignol, R. Ferreira, and J.-M. Gérard, Nat. Phys. **2**, 759 (2006).

[40] C. Santori, D. Fattal, J. Vučković, G. S. Solomon, and Y. Yamamoto, Nature (London) **419**, 594 (2002).

[41] J. Bylander, I. Robert-Philip, and I. Abram, Eur. Phys. J. D **22**, 295 (2003).

[42] P. Gold, A. Thoma, S. Maier, S. Reitzenstein, C. Schneider, S. Höfling, and M. Kamp, Phys. Rev. B **89**, 035313 (2014).

[43] M. Delbecq, T. Nakajima, P. Stano, T. Otsuka, S. Amaha, J. Yoneda, K. Takeda, G. Allison, A. Ludwig, A. Wieck *et al.*, Phys. Rev. Lett. **116**, 046802 (2016).

[44] C. Arnold, V. Loo, A. Lemaître, I. Sagnes, O. Krebs, P. Voisin, P. Senellart, and L. Lanco, Phys. Rev. X **4**, 021004 (2014).

[45] H. Wang, Z. C. Duan, Y. H. Li, S. Chen, J. P. Li, Y. M. He, M. C. Chen, Y. He, X. Ding, C. Z. Peng, C. Schneider, M. Kamp, S. Höfling, C. Y. Lu, and J. W. Pan, Phys. Rev. Lett. **116**, 213601 (2016).

[46] G. D. Mahan, *Many-Particle Physics* (Springer, New York, 2013).

[47] C. Cohen-Tannoudji, J. Dupont-Roc, G. Grynberg, and P. Thickstun, *Atom-Photon Interactions: Basic Processes and Applications* (Wiley Online Library, New York, 1992).

[48] K. Roy-Choudhury and S. Hughes, Phys. Rev. B **92**, 205406 (2015).

[49] This is a manifold of three degenerate states with p symmetry.

[50] The value of $\mathcal{F}$ varies between 0.19 for $T \sim 4$ K and 0.33 for $T \sim 22$ K.